



Comparison of the neutronic properties of the $(\text{Th-}^{233}\text{U})\text{O}_2$, $(\text{Th-}^{233}\text{U})\text{C}$, and $(\text{Th-}^{233}\text{U})\text{N}$ fuels in small long-life PWR cores with 300, 400, and 500 MW_{th} of power

Boni Pahlanop Lapanporo ,
Zaki Su'ud ,
Asril Pramutadi Andi Mustari

Abstract. The neutronic characteristics of $(\text{Th-}^{233}\text{U})\text{O}_2$, $(\text{Th-}^{233}\text{U})\text{C}$, and $(\text{Th-}^{233}\text{U})\text{N}$ have been compared in small long-life pressurized water reactors (PWRs). Neutronic calculations were carried out at 300 MW_{th} , 400 MW_{th} , and 500 MW_{th} with two cladding types: zircaloy-4 and ZIRLO (Zr low oxygen). They were performed using the Standard Reactor Analysis Code (SRAC) and JENDL-4.0 nuclide data, dividing the reactor core into three fuel zones with varying ^{233}U enrichment levels, ranging from 3% to 9% and fluctuating by 1%, employing the PIJ module at the fuel cell level and the CITATION module at the reactor core level. In addition, ^{251}Pa was added as burnable poison (BP). The $(\text{Th-}^{233}\text{U})\text{N}$ fuel demonstrated superior criticality compared to the other fuel types, as it consistently achieves critical conditions throughout the reactor's operating cycle with excess reactivity $< 1.00\%$ dk/k for several fuel configurations at the 300 MW_{th} and 400 MW_{th} power levels. Moreover, the $(\text{Th-}^{233}\text{U})\text{N}$ and $(\text{Th-}^{233}\text{U})\text{C}$ fuels exhibited similar and flatter power density distribution patterns compared to the $(\text{Th-}^{233}\text{U})\text{O}_2$ fuel. The power peaking factor (PPF) value was relatively higher for $(\text{Th-}^{233}\text{U})\text{O}_2$ fuel than the other two fuels. The $(\text{Th-}^{233}\text{U})\text{N}$ fuel exhibited the most negative Doppler coefficient, followed by $(\text{Th-}^{233}\text{U})\text{C}$ and $(\text{Th-}^{233}\text{U})\text{O}_2$ fuels. Analysis of burnup levels revealed that the $(\text{Th-}^{233}\text{U})\text{O}_2$ fuel achieved significantly higher burnup than the other two fuels.

Keywords: CITATION • Core design • Long-life PWR • SMR • SRAC • Thorium

B. P. Lapanporo
Department of Physics, Faculty of Mathematics
and Natural Sciences, Institut Teknologi Bandung
Jl. Ganesa 10, Bandung 40132, Indonesia
and Department of Physics, Faculty of Mathematics
and Natural Sciences, Universitas Tanjungpura, Jl. Prof.
Dr. H. Hadari Nawawi, Pontianak 78124, Indonesia

Z. Su'ud , A. P. A. Mustari
Department of Physics, Faculty of Mathematics
and Natural Sciences, Institut Teknologi Bandung
Jl. Ganesa 10, Bandung 40132, Indonesia
and Nuclear Physics & Biophysics Research Division
Department of Physics, Faculty of Mathematics
and Natural Sciences, Institut Teknologi Bandung
Jl. Ganesa 10, Bandung 40132, Indonesia
E-mail: szaki@fi.itb.ac.id

Received: 3 April 2023
Accepted: 14 December 2023

Introduction

Energy consumption is experiencing rapid growth globally, driven by increasing population and economic development. To satisfy this energy need, it is necessary to introduce an alternate energy source that is cleaner and more reliable, i.e., nuclear energy. In 2018, nuclear energy accounted for around 10% of the world's electricity generation [1].

The pressurized water reactor (PWR) is the most common type of nuclear reactor used for power generation and is used on navy ships, such as submarines, aircraft carriers, and icebreakers [2]. Currently, the development of PWR as a power plant has also progressed toward developing small modular long-life reactors with small-medium power levels to reach remote areas and produce a more even energy distribution system [3].

Over the last few decades, UO_2 fuel has been widely used as an energy source in light water reactors (LWRs) in one fuel cycle. The high level of uranium consumption caused the natural resources of this fuel to be limited until this century despite the increase in the price of uranium ore [4]. Re-fabrication of the fuel can be done to keep using

the uranium-based fuel in the long run. However, this procedure entails higher expenditures, burdening nations that employ nuclear energy in the future [5]. In addition to the limited quantity, uranium will produce byproducts such as plutonium and various minor actinides, which are long-lived, so alternate nuclear fuels are required. One of them is to use fuel derived from thorium [6].

Using thorium as a nuclear fuel has many advantages compared to uranium-based fuels. Among them, it is 3–4 times more abundant than uranium, has a higher conversion ratio than ^{235}U and ^{239}Pu , and has a lower formation of minor actinides [7, 8]. Chemically, thorium is also more stable than uranium and can withstand higher combustion [9]. The high conversion ratio of thorium-based fuel causes this fuel to be very potent if used as a long-life reactor fuel without refueling in a place based on a thermal neutron spectrum, such as in a PWR [10]. To produce energy in a thermal reactor, thorium, which consists of the single isotope ^{232}Th , must be converted to a fissile isotope. The fissile isotope formed is ^{235}U through converting ^{232}Th to ^{233}Th and ^{233}Pa . For this process to occur, sufficient fissile material must be in the reactor core. Fissile isotopes can be prepared separately or homogeneously mixed with thorium [11, 12]. Due to the greater absorption cross-section of ^{232}Th , the generation of ^{235}U accelerates with an increasing starting mass of ^{232}Th [13].

In recent years, much research on the utilization of thorium-based fuel in PWR cores has been conducted: Uguru *et al.* [14] investigated the impact of ^{238}U fuel replacement on the fuel matrix of the Westinghouse small modular PWR, using thorium-based fuel with different enrichment levels. Gorton *et al.* [8] conducted an analysis comparing the fuel cycle length, reactivity coefficient, and thermal margin safety of ThN–UN fuel to UO_2 under normal operating conditions of a PWR. du Toit and Naicker [6] examined the utilization of ThO_2 fuel in the European pressurized reactor (EPR) core for a 24-month fuel cycle, employing MCNP6 for their analysis. Galahom *et al.* [15] explored the potential benefits of using thorium-based PWR fuel from a neutron analysis perspective. Oettingen and Skolik [16] focused on designing a numerical seed-blanket unit for thorium nuclear fuel cycles in the PWR 17×17 fuel assembly designed according to the Radkowsky thorium fuel concept.

Additionally, more research on the properties of thorium-based fuels used in PWR cores has been conducted: Liu *et al.* [17] modeled the performance of $(\text{Th}, \text{U})\text{O}_2$ and $(\text{Th}, \text{Pu})\text{O}_2$ fuels with SiC cladding consisting of two layers using multiphysics simulations. Castro *et al.* [18] investigated the depletion and criticality of thorium-added recycled fuel in a PWR core. Tucker and Usman [19] analyzed the combustion of mixed thorium–plutonium oxide (ThMOX) fuel in a PWR core, employing the Monte Carlo N-Particle (MCNP) code. Maiorino *et al.* [20] conducted a feasibility study on the neutronic and thermal-hydraulic aspects of converting UO_2 fuel to $(\text{U-Th})\text{O}_2$ in a PWR core through a parametric analysis. Zainuddin *et al.* [21] examined the factors

influencing the moderator temperature coefficient (MTC) in PWRs fueled with thorium–plutonium. Morrison *et al.* [22] explored the relationship between Doppler reactivity and integral resonance for thorium and uranium fuels in PWR cores. Li *et al.* [23] analyzed the feasibility and neutronic characteristics of a micro-heterogeneous duplex pin fuel with ThO_2 – UO_2 in PWR cores.

In this study, neutronic calculations were carried out for thorium-based fuels with a mixture of ^{235}U fissile materials on long-life PWR cores with 300 MW_{th} , 400 MW_{th} , and 500 MW_{th} power. Th– ^{235}U fuel is a practical combination that can reproduce independently in the LWR core in the thermal spectrum because it has an η -factor (number of fission neutrons released per neutron absorbed) that is relatively >2 in the thermal spectrum [24]. In this study, three types of fuel were used, namely $(\text{Th-}^{235}\text{U})\text{O}_2$, $(\text{Th-}^{235}\text{U})\text{C}$, and $(\text{Th-}^{235}\text{U})\text{N}$, which are dioxide, carbide, and nitride, respectively. The cladding materials used for these three fuel types are zircaloy-4 and ZIRLO. This study is essential to understand the neutronic characteristics of these three fuels with zircaloy-4 and ZIRLO cladding when utilized in long-life PWR cores. Several parameters were examined to determine the neutronic performance of these three fuels, including effective multiplication factor (k_{eff}), excess reactivity, power density distribution, power peaking factor (PPF), fuel temperature (Doppler) coefficient, and burnup level.

Methodology

Reactor design

The geometry of the fuel cell used in the analyzed PWR is square, as shown in Fig. 1, with a pitch diameter of 1.4 cm, a cladding thickness of 0.057 cm, and a 60% fuel volume fraction. The fuel used is Th– ^{235}U , with the types of dioxide, carbide, and nitride. Two types of cladding are used in this study, namely zircaloy-4 and ZIRLO (Zr low oxygen). Both are cladding zirconium-based alloys commonly used in PWR, with almost the same composition, but ZIRLO exhibits superior mechanical properties and

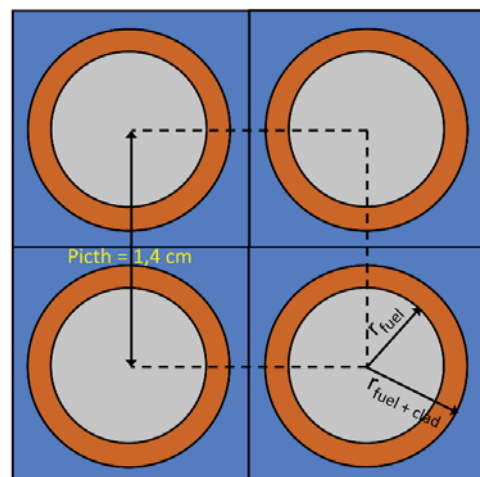


Fig. 1. Fuel cell design.

enhanced corrosion resistance compared to zircaloy-4 [25]. The height and diameter of the PWR under analysis are 240.8 cm and 224.0 cm, respectively, and it has three different power levels: 300 MW_{th}, 400 MW_{th}, and 500 MW_{th}. These power levels have power densities of 31.63 W/cc, 42.17 W/cc, and 52.72 W/cc, respectively. When compared to the average core power density of the conventional PWR AP1000 (109.7 W/cc) [26], each of these power levels represents approximately 28.83%, 38.44%, and 48.06% of the AP1000's power density. This reactor's design uses lower power levels to enable extended reactor operation.

The reflector is made of stainless steel and water, and it has a 22.4 cm thickness. The reactor core has three fuel regions (F1, F2, and F3) with a 1% ²³⁵U content difference between each fuel region. F1 is the fuel region with the least fissile material, F2 is the fuel region with the medium fissile material, and F3 is the fuel region with the most fissile material [27]. The analyzed PWR design parameters are shown in Table 1. For the reactor core calculations in this study, a two-dimensional R-Z geometry is used, divided into three radial and axial fuel regions with different ²³⁵U enrichments, as shown in Fig. 2. In the radial direction, F1 and F2 each have a radius of 39.2 cm, while F3 has a radius of 33.6 cm. In the axial direction, F1 has a radius of 42 cm, while F2 and F3 each have a radius of 39.2 cm.

Table 1. Design parameters of small long-life PWR

Parameters	Specification
Thermal power reactors	300, 400, 500 MW _{th}
Fuel	(Th- ²³⁵ U)O ₂ , (Th- ²³⁵ U)C, (Th- ²³⁵ U)N
Cladding structure	Zircaloy-4 and ZIRLO
Coolant	H ₂ O
Reflector	Stainless steel and H ₂ O
Geometry of fuel cell	Square cell
Percentage enrichment of ²³⁵ U	3–9%
Smear density	85%
Fuel volume fraction	60%
Cladding density	6.5 g/cm ³
Cladding thickness	0.057 cm
Coolant density	0.72 g/cm ³
Pin pitch	1.4 cm
Diameter of active core	224.0 cm
Height of active core	240.8 cm

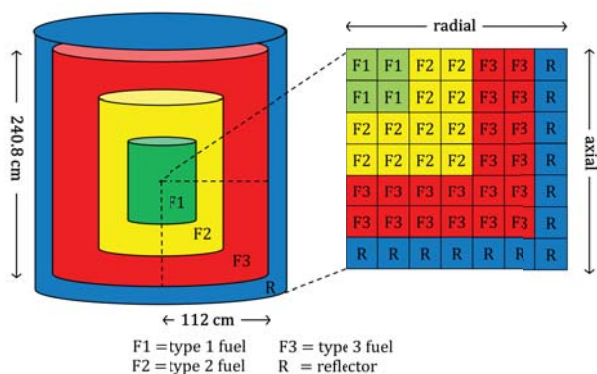


Fig. 2. Small long-life PWR core design.

Table 2. The neutron energy group used in the calculation

Spectrum type	Group	Energy range (eV)		
		Upper	Lower	
Fast neutron	1	1.000×10^7	1.855×10^0	
	Thermal neutron	2	1.855×10^0	8.764×10^{-1}
		3	8.764×10^{-1}	4.139×10^{-1}
		4	4.139×10^{-1}	2.770×10^{-1}
		5	2.770×10^{-1}	1.674×10^{-1}
		6	1.674×10^{-1}	8.529×10^{-2}
		7	8.529×10^{-2}	3.060×10^{-2}
		8	3.060×10^{-2}	1.000×10^{-5}

Calculation method

Calculations are performed using the Standard Reactor Analysis Code (SRAC). The fuel cell level calculations are performed using the PIJ module based on the collision probability method (CPM). Subsequently, the macroscopic cross-section values of the fuel are obtained at each burnup step. These values are then used to solve the multigroup diffusion equations using CITATION for the PWR core level. The SRAC system facilitates neutron calculations for different thermal reactors by generating accurate microscopic and macroscopic cross-sections. It supports core and static cell calculations, including burnup analysis, and provides essential parameters for reactor design and experimental analysis [27]. As a nuclear data library, we utilize JENDL 4.0.

Thermal neutrons support the fission reaction taking place in the PWR core. There are 107 neutron energy group structures in the SRAC module, with 74 fast neutron energy groups, 48 thermal neutron energy groups, and 15 overlapping groups [28]. In this calculation, the neutron group is condensed into eight neutron energy groups, which consist of a fast neutron energy group and seven thermal neutron energy groups, as shown in Table 2.

In Fig. 2, the fuel configuration (F1, F2, and F3) used in the core consists of five variations of ²³⁵U enrichment configurations, i.e., 3–4–5%, 4–5–6%, 5–6–7%, 6–7–8%, and 7–8–9%. In each fuel cell, ²³¹Pa is added as a burnable poison (BP). ²³¹Pa is not only able to reduce excess reactivity but can also increase fuel burnup [29]. For each fuel configuration, ²³¹Pa is randomly added between 0.20% and 7.45% with a minimum increment of 0.05%. Neutronic calculations aim to see which fuel configuration has an optimum criticality level or effective multiplication factor (k_{eff}) with excess reactivity not exceeding 1.00% dk/k for a minimum burnup period of up to 20 years. Other neutronic aspects also considered are power density distribution, PPF, fuel temperature (Doppler) coefficient, and burnup level for the three fuel types.

Results and discussion

Effective multiplication factor (k_{eff})

Neutronic calculations were carried out for the three types of dioxide, carbide, and nitride fuels,

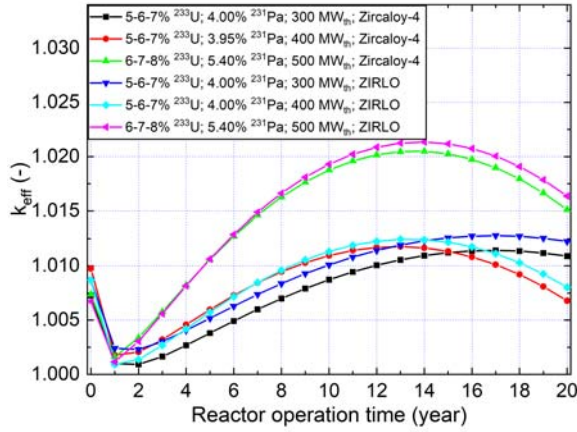


Fig. 3. The effective multiplication factor (k_{eff}) for small long-life PWR with $(\text{Th}^{235}\text{U})\text{O}_2$ fuel.

for two types of cladding, zircaloy-4 and ZIRLO, and for power levels of 300 MW_{th} , 400 MW_{th} , and 500 MW_{th} , with variations in the addition of ^{231}Pa as BP randomly between 0.20% and 7.45% with a minimum difference of 0.05%. Figure 3 shows the results of the k_{eff} calculation for the $(\text{Th}^{235}\text{U})\text{O}_2$ fuel configuration.

Figure 3 shows that for the $(\text{Th}^{235}\text{U})\text{O}_2$ fuel type, no fuel configuration reaches a critical condition throughout the reactor operation cycle with excess reactivity $< 1.00\%$ dk/k. Both for the zircaloy-4 and the ZIRLO cladding types, the best performance is

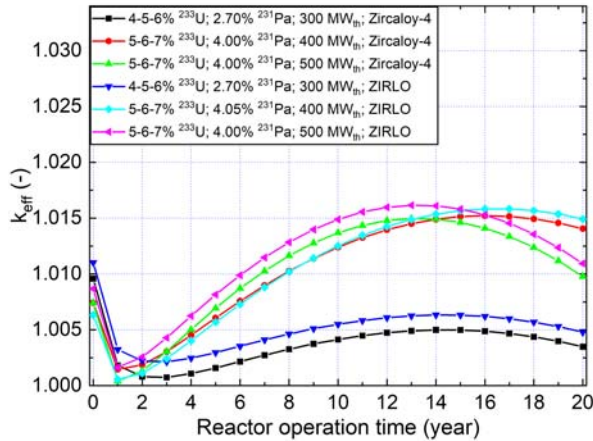


Fig. 4. The effective multiplication factor (k_{eff}) for small long-life PWR with $(\text{Th}^{235}\text{U})\text{C}$ fuel.

Table 3. Excess reactivity for all types of fuel with the best level of criticality

Fuel	$\%^{235}\text{U}$	$\%^{231}\text{Pa}$	Cladding	Power (MW_{th})	Excess reactivity (% dk/k)		
					BOC	EOC	Maximum
$(\text{Th}^{235}\text{U})\text{O}_2$	5–6–7	4.00	Zircaloy-4	300	0.72	1.08	1.13
$(\text{Th}^{235}\text{U})\text{O}_2$	5–6–7	3.95	Zircaloy-4	400	0.96	0.80	1.16
$(\text{Th}^{235}\text{U})\text{O}_2$	5–6–7	4.00	ZIRLO	300	0.86	1.21	1.26
$(\text{Th}^{235}\text{U})\text{O}_2$	5–6–7	4.00	ZIRLO	400	0.86	0.92	1.23
$(\text{Th}^{235}\text{U})\text{C}$	4–5–6	2.70	Zircaloy-4	300	0.95	0.40	0.95
$(\text{Th}^{235}\text{U})\text{C}$	4–5–6	2.70	ZIRLO	300	1.09	0.53	1.09
$(\text{Th}^{235}\text{U})\text{N}$	6–7–8	4.35	Zircaloy-4	300	0.65	0.22	0.65
$(\text{Th}^{235}\text{U})\text{N}$	6–7–8	4.35	Zircaloy-4	400	0.65	0.01	0.65
$(\text{Th}^{235}\text{U})\text{N}$	7–8–9	6.05	Zircaloy-4	300	0.32	0.99	0.99
$(\text{Th}^{235}\text{U})\text{N}$	6–7–8	4.35	ZIRLO	300	0.76	0.32	0.76
$(\text{Th}^{235}\text{U})\text{N}$	6–7–8	4.35	ZIRLO	400	0.76	0.10	0.76
$(\text{Th}^{235}\text{U})\text{N}$	7–8–9	6.05	ZIRLO	300	0.41	1.08	1.08

BOC, beginning of cycle; EOC, end of cycle.

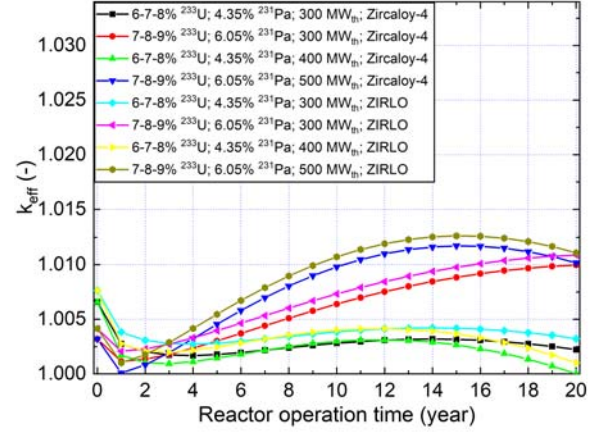


Fig. 5. The effective multiplication factor (k_{eff}) for small long-life PWR with $(\text{Th}^{235}\text{U})\text{N}$ fuel.

achieved with an enrichment configuration of 5–6–7% ^{235}U at power levels of 300 MW_{th} and 400 MW_{th} , with excess reactivity slightly exceeding 1.00% dk/k.

For fuel $(\text{Th}^{235}\text{U})\text{C}$, the optimal fuel performance is achieved with an enrichment configuration of 4–5–6% ^{235}U for both cladding types at a 300 MW_{th} power level. As shown in Fig. 4 for the zircaloy-4 cladding type, the fuel configuration 4–5–6% ^{235}U reaches a critical condition with excess reactivity $< 1.00\%$ dk/k until the 20th year. For fuel $(\text{Th}^{235}\text{U})\text{C}$ with 4–5–6% ^{235}U with a ZIRLO cladding type, critical conditions with excess reactivity close to 1.00% dk/k throughout the cycle up to the 20th year are possible.

Figure 5 shows that for $(\text{Th}^{235}\text{U})\text{N}$ fuel with an enrichment configuration of 6–7–8% ^{235}U for both cladding types at power levels of 300 MW_{th} and 400 MW_{th} , it can achieve a critical condition throughout the reactor operation cycle with excess reactivity $< 1.00\%$ dk/k. Furthermore, the fuel configuration of 7–8–9% ^{235}U for zircaloy-4 cladding type at a power level of 300 MW_{th} also maintains excess reactivity $< 1.00\%$ dk/k throughout the reactor operation cycle. However, the fuel configuration of 7–8–9% ^{235}U for the ZIRLO cladding type at a power level of 300 MW_{th} has the maximum excess reactivity value slightly exceeding 1.00% dk/k.

The excess reactivity for the three fuel types with the best criticality levels for various configurations of ^{235}U enrichment is shown in Table 3. These values

are displayed at the beginning of cycle (BOC) and the end of cycle (EOC) conditions. The maximum value of excess reactivity throughout the reactor operation cycle is also presented.

Based on the conducted neutronic calculations, it was observed that reaching a critical condition of up to 20 years is a challenge for (Th-²³³U)O₂ and (Th-²³³U)C fuels with a ²³³U enrichment configuration of 3–4–5%. Reducing the percentage of BP in this configuration causes higher excess reactivity at BOC. However, the k_{eff} value decreases sharply as the reactor operating time increases due to the depletion of fissile material. This condition is also observed in the (Th-²³³U)N fuel with ²³³U enrichment configurations of 3–4–5% and 4–5–6% in the reactor core.

Comparing the three fuel types, it is evident that the (Th-²³³U)N fuel exhibits the best performance regarding reactor criticality. In the (Th-²³³U)N fuel, two fuel configurations within the reactor core consistently maintain critical conditions throughout the operating cycle, with excess reactivity < 1.00% dk/k. However, due to its higher density, achieving critical conditions throughout the operating cycle requires more fissile material for the (Th-²³³U)N fuel than the other two fuel types. Additionally, the neutronic calculations indicate that ZIRLO cladding yields a slightly higher k_{eff} value than the zircaloy-4 cladding type.

Power density

The power density distribution pattern for the three types of fuel with the best criticality is shown in Figs. 6–8, each for the power distribution pattern in the radial direction and the power distribution pattern in the axial direction obtained based on the calculation results using the SRAC code with the CITATION module. From Figs. 6–8, it can be seen that for both zircaloy-4 and ZIRLO claddings, the power density distribution pattern for the three types of fuel has the same shape, both in the radial and axial directions.

In Figs. 6a, 7a, and 8a, a similar pattern of power density distribution is observed for the three fuel types. The radial power density distribution is nearly identical for the BOC and middle of cycle (MOC) near the center of the reactor core. However, beyond a distance of 81.44 cm from the core's center, the power density at the MOC tends to resemble the density at the EOC. The peak power density in the radial direction occurs near the core for BOC, MOC, and EOC. In the radial direction, it can be seen that the power density distribution for (Th-²³³U)C and (Th-²³³U)N fuels is more uniform compared to (Th-²³³U)O₂ fuel during BOC and MOC.

In the axial direction, as shown in Figs. 6b, 7b, and 8b, the distribution patterns for the three fuel types also exhibit similarities. In the axial direction, it can be observed that all three fuels have significant

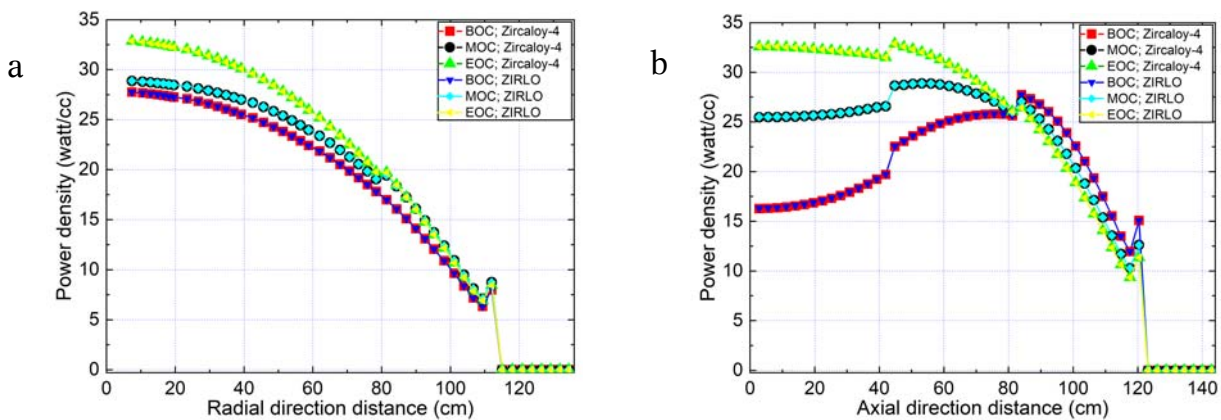


Fig. 6. Power density distribution for (Th-²³³U)O₂ fuel at 5–6–7% ²³³U, 4.00% ²³¹Pa, and 300 MW_{th}. (a) Radial direction, (b) axial direction (1 mesh = 2.80 cm).

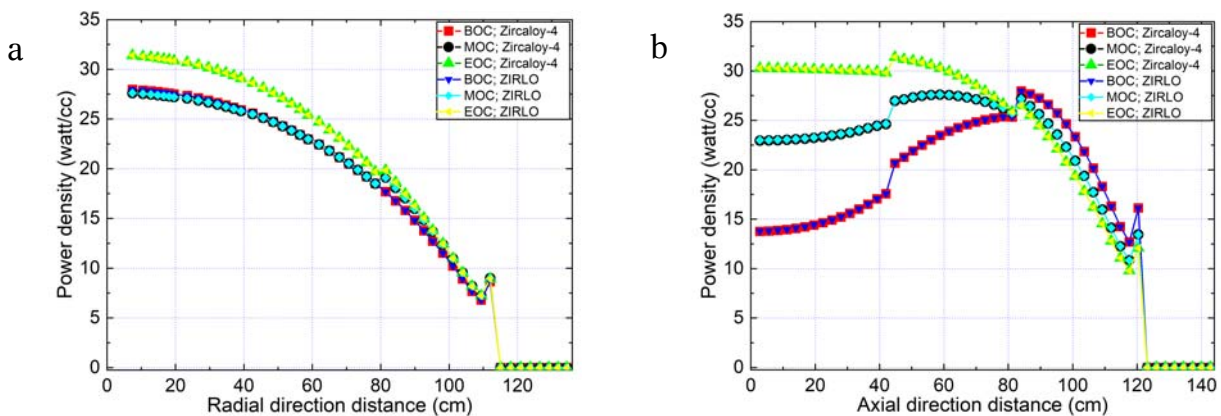


Fig. 7. Power density distribution for (Th-²³³U)C fuel at 4–5–6% ²³³U, 2.70% ²³¹Pa, and 300 MW_{th}. (a) Radial direction, (b) axial direction (1 mesh = 2.80 cm).

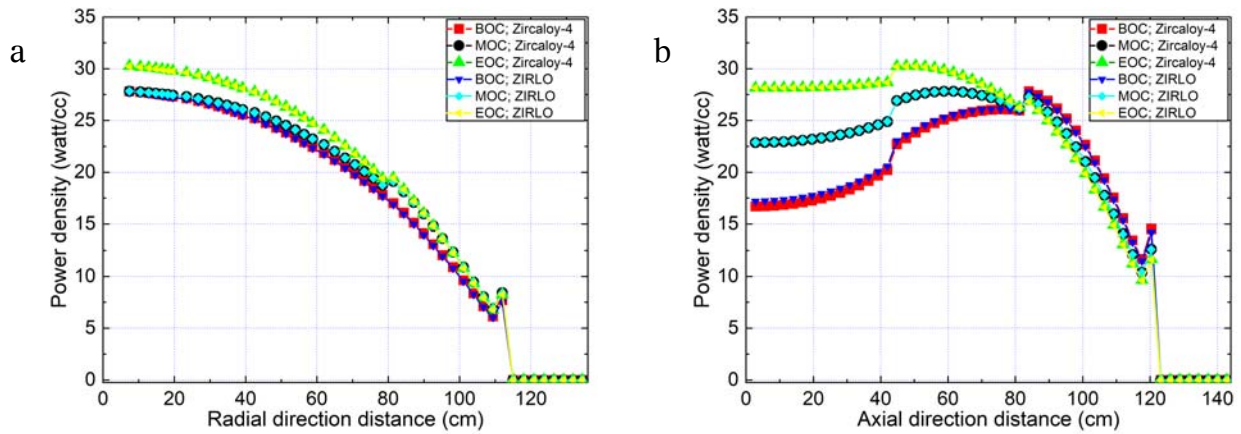


Fig. 8. Power density distribution for (Th-²³⁵U)N fuel at 6–7–8% ²³⁵U, 4.35% ²³¹Pa, and 300 MW_{th}. (a) Radial direction, (b) axial direction (1 mesh = 2.80 cm).

Table 4. The peak power density (watt/cc) for all types of fuel with the best level of criticality

Fuel	% ²³⁵ U	% ²³¹ Pa	Cladding	Power (MW _{th})	BOC		MOC		EOC	
					Radial	Axial	Radial	Axial	Radial	Axial
(Th- ²³⁵ U)O ₂	5–6–7	4.00	Zircaloy-4	300	27.75	27.75	28.87	28.87	32.86	32.58
(Th- ²³⁵ U)O ₂	5–6–7	4.00	ZIRLO	300	27.75	27.75	28.88	28.88	32.88	32.61
(Th- ²³⁵ U)C	4–5–6	2.70	Zircaloy-4	300	27.97	27.97	27.59	27.59	31.39	31.39
(Th- ²³⁵ U)C	4–5–6	2.70	ZIRLO	300	27.96	27.96	27.60	27.60	31.40	31.40
(Th- ²³⁵ U)N	6–7–8	4.35	Zircaloy-4	300	27.82	27.82	27.82	27.82	30.27	30.27
(Th- ²³⁵ U)N	6–7–8	4.35	ZIRLO	300	27.74	27.74	27.83	27.83	30.24	30.24

BOC, beginning of cycle; EOC, end of cycle; MOC, middle of cycle.

variations in power density near the axial center up to a distance of approximately 81.20 cm during BOC, MOC, and EOC.

The differences in power density distribution under BOC, MOC, and EOC for the three fuel types are more significantly pronounced in the axial direction, suspected to be due to the more substantial disparity in neutron flux along the axial direction. On average, the power density at EOC is greater than at MOC and BOC due to the maximum fuel burnup condition at EOC. In the power density distribution, three peaks of power density delineate the boundaries between fuel regions F1 and F2, F2 and F3, and F3 and the reflector. The peaks of power density that emerge between the boundaries of fuel regions occur because there is a change in the density of the fuel material at these fuel region boundaries. At the boundaries between fuel regions F1 and F2, as well as F2 and F3, there are variations in material density due to an increase in the enrichment of ²³⁵U, which naturally leads to an increase in the number of fission reactions, thus resulting in the appearance of power density peaks at these fuel region boundaries. Meanwhile, the power density peak occurring between the boundary of fuel region F3 and the reflector is caused by neutron reflection in this area. This reflection results in an increase in the number of thermal neutrons at this boundary, inevitably causing an increase in the number of fission reactions and generating a power density peak.

It can be seen that the difference in power density distribution under BOC, MOC, and EOC conditions is only significant up to a distance of 81.20 cm from the center of the reactor core, which marks the boundary between the fuel regions F2 and F3. This

condition is caused in the F3 fuel region with the highest enrichment level of ²³⁵U; there is a greater decrease in the k_{eff} value as the reactor operating time increases when compared to the other two fuel regions causing a greater decrease in power density at the time of MOC and EOC for this fuel region.

The peak power density of the three fuel types shown in Figs. 6–8 is indicated in Table 4. These peaks are displayed under BOC, MOC, and EOC conditions. It can be seen that the peak power density in both the radial and axial directions has the same value.

Power peaking factor

The PPF is the maximum local power density ratio to the average power density [30]. PPF is an important parameter that must be known to avoid fuel rod melting and violation of safety limits [31]. A smaller PPF will lead to more uniform fuel depletion and more even coolant distribution in the radial and axial directions, which can result in the reactor core using fuel more efficiently [32]. Table 5 shows the PPF value for the fuel with the best criticality level. The PPF values for the three fuel types do not significantly differ. The PPF value in the radial direction tends to be greater than the PPF value in the axial direction. During BOC, the PPF value in the radial direction for fuel (Th-²³⁵U)N tends to be greater than the PPF value for the other two types of fuel, while in the axial direction, the PPF value when BOC for fuel (Th-²³⁵U)C tends to be more significant. At MOC, the PPF value of (Th-²³⁵U)O₂ fuel tends to be greater than the PPF value of the

Table 5. Power peaking factor for all types of fuel with the best level of criticality

Fuel	% ²³⁵ U	% ²³¹ Pa	Cladding	Power (MW _{th})	BOC		MOC		EOC	
					Radial	Axial	Radial	Axial	Radial	Axial
(Th- ²³⁵ U)O ₂	5-6-7	4.00	Zircaloy-4	300	1.644	1.323	1.573	1.185	1.698	1.223
(Th- ²³⁵ U)O ₂	5-6-7	3.95	Zircaloy-4	400	1.645	1.321	1.586	1.195	1.662	1.277
(Th- ²³⁵ U)O ₂	6-7-8	5.40	Zircaloy-4	500	1.669	1.271	1.648	1.211	1.732	1.319
(Th- ²³⁵ U)O ₂	5-6-7	4.00	ZIRLO	300	1.645	1.322	1.574	1.185	1.698	1.223
(Th- ²³⁵ U)O ₂	5-6-7	4.00	ZIRLO	400	1.645	1.322	1.587	1.196	1.665	1.279
(Th- ²³⁵ U)O ₂	6-7-8	5.45	ZIRLO	500	1.669	1.272	1.649	1.211	1.734	1.320
(Th- ²³⁵ U)C	4-5-6	2.70	Zircaloy-4	300	1.631	1.334	1.551	1.182	1.638	1.208
(Th- ²³⁵ U)C	5-6-7	4.00	Zircaloy-4	400	1.631	1.333	1.586	1.184	1.587	1.235
(Th- ²³⁵ U)C	5-6-7	4.00	Zircaloy-4	500	1.631	1.333	1.588	1.195	1.667	1.283
(Th- ²³⁵ U)C	4-5-6	2.70	ZIRLO	300	1.631	1.333	1.552	1.182	1.638	1.208
(Th- ²³⁵ U)C	5-6-7	4.05	ZIRLO	400	1.631	1.333	1.587	1.184	1.589	1.236
(Th- ²³⁵ U)C	5-6-7	4.00	ZIRLO	500	1.632	1.332	1.589	1.195	1.667	1.283
(Th- ²³⁵ U)N	6-7-8	4.35	Zircaloy 4	300	1.649	1.311	1.580	1.185	1.657	1.211
(Th- ²³⁵ U)N	6-7-8	4.35	Zircaloy 4	400	1.649	1.311	1.602	1.188	1.573	1.224
(Th- ²³⁵ U)N	7-8-9	6.05	Zircaloy 4	500	1.667	1.274	1.599	1.190	1.589	1.231
(Th- ²³⁵ U)N	6-7-8	4.35	ZIRLO	300	1.650	1.311	1.580	1.185	1.658	1.211
(Th- ²³⁵ U)N	6-7-8	4.35	ZIRLO	400	1.650	1.311	1.602	1.188	1.575	1.225
(Th- ²³⁵ U)N	7-8-9	6.05	ZIRLO	500	1.667	1.273	1.600	1.191	1.590	1.232

BOC, beginning of cycle; EOC, end of cycle; MOC, middle of cycle.

other two fuel types in the radial and axial directions. During EOC, the PPF value of (Th-²³⁵U)O₂ fuel also tends to be greater than the PPF value of the other two fuel types, both in the radial and axial directions. From these results, it can be seen that fuel (Th-²³⁵U)O₂ has a relatively higher PPF value when compared to the other two fuel types, while fuels (Th-²³⁵U)C and (Th-²³⁵U)N tend to have PPF values as relatively the same. Generally, PPF values for all fuel types are still within safe limits for PWR-type reactors, with values below two.

Fuel temperature (Doppler) coefficient

The fuel temperature (Doppler) coefficient is the reactivity change per degree change in the average core fuel temperature. Reactors are typically constructed with a negative Doppler coefficient to assist control so that if a power excursion occurs, the negative reactivity will be fed back into the system [33]. We calculated the Doppler coefficient by increasing the fuel temperature by 100°C in the fuel cell calculation using the PIJ module in the SRAC code, then compared the reactivity obtained from the neutronic calculation using the CITATION module on the reactor core with the reactivity before the temperature increase. The Doppler coefficient for the three fuel types with the best performance level at each power level and type of cladding used is shown in Figs. 9–11. The calculation results show that the Doppler coefficient values for the three fuel types have the same pattern, with the most negative values occurring at the beginning of the reactor operating time and then less negative until the end. The less negative value of the Doppler coefficient is due to the reduced reactivity value as the reactor operating time increases.

Figure 9 shows the change in the Doppler coefficient value with increasing reactor operating time

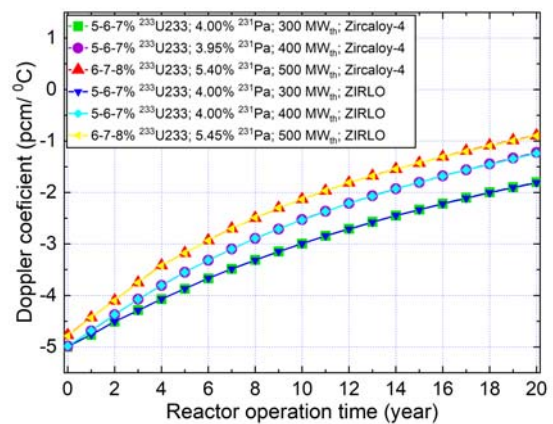


Fig. 9. Doppler coefficient for the (Th-²³⁵U)O₂ fuel with the best criticality at 300 MW_{th}, 400 MW_{th}, and 500 MW_{th} with zircaloy-4 and ZIRLO cladding.

for fuel (Th-²³⁵U)O₂ with the best criticality level. The Doppler coefficient is relatively the same for fuels using zircaloy-4 and ZIRLO cladding. The average value of the Doppler coefficient of fuel (Th-²³⁵U)O₂ with the best criticality level is -2.94 pcm/°C at 300 MW_{th} power level, -2.77 pcm/°C at 400 MW_{th} power level, and -2.57 pcm/°C at a power level of 500 MW_{th}.

Figure 10 illustrates the variation of the Doppler coefficient value over reactor operating time for the fuel (Th-²³⁵U)C, which exhibits the best criticality level. Similar to (Th-²³⁵U)O₂ fuel, the Doppler coefficient value remains relatively consistent for both zircaloy-4 and ZIRLO cladding. The average Doppler coefficient for (Th-²³⁵U)C fuel is -3.15 pcm/°C at a power level of 300 MW_{th}, -3.00 pcm/°C at 400 MW_{th}, and -2.77 pcm/°C at 500 MW_{th}.

Figure 11 shows the change in the Doppler coefficient value with increasing reactor operating time for fuel (Th-²³⁵U)N at the best criticality level. In contrast to the other two fuel types, the Doppler

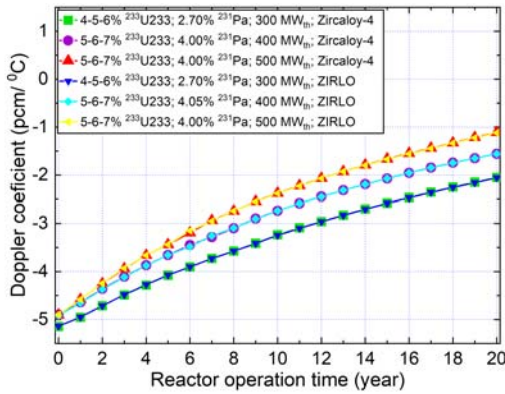


Fig. 10. Doppler coefficient for the (Th-²³⁵U)C fuel with the best criticality at 300 MW_{th}, 400 MW_{th}, and 500 MW_{th} with zircaloy-4 and ZIRLO cladding.

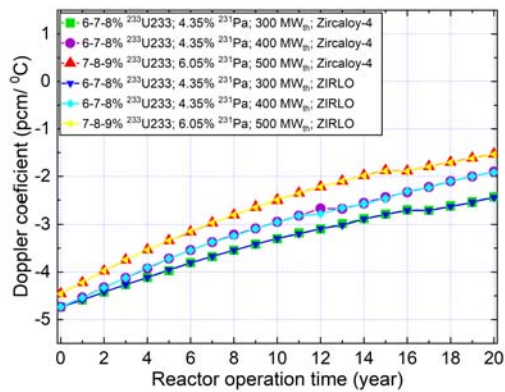


Fig. 11. Doppler coefficient for the (Th-²³⁵U)N fuel with the best criticality at 300 MW_{th}, 400 MW_{th}, and 500 MW_{th} with zircaloy-4 and ZIRLO cladding.

coefficient is relatively the same for using zircaloy-4 and ZIRLO cladding for all power levels. However, there are several shifts at several points in the cycle time of reactor operation. At the BOC, the Doppler coefficient for (Th-²³⁵U)N fuel is less negative than the other two types of fuels, but at the EOC, this fuel exhibits a more negative Doppler coefficient than the other two fuels. The average Doppler coefficient of fuel (Th-²³⁵U)N is -3.32 pcm/°C at 300 MW_{th} power level, -3.17 pcm/°C at 400 MW_{th} power level, and -2.95 pcm/°C at 500 power level MW_{th}.

The calculations show that the Doppler coefficient tends to be less negative as the reactor power increases. The three fuel types have negative Doppler coefficient values from the beginning to the end of the reactor operating time. This negative Doppler coefficient value is important for the reactor to preserve its inherent safety characteristics during fast changes in the reactor core power [34]. On average, it can be seen that the most negative Doppler coefficient is found in fuel (Th-²³⁵U)N, followed by fuel (Th-²³⁵U)C and (Th-²³⁵U)O₂.

Burnup level

Figures 12–14 show the burnup levels for the three fuel types at power levels 300 MW_{th}, 400 MW_{th}, and 500 MW_{th}. From the calculations, the concentration of fissile material ²³⁵U, ²³¹Pa as burnable poison (BP), and the type of cladding used had no significant

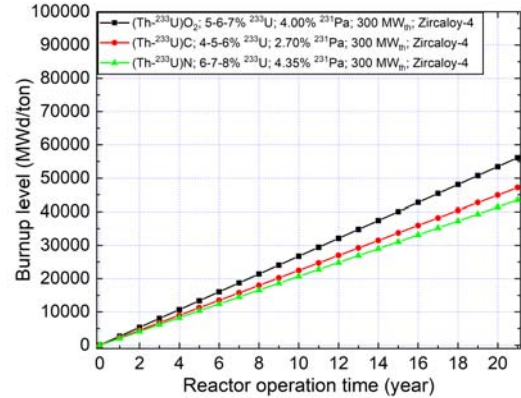


Fig. 12. Burnup level of (Th-²³⁵U)O₂, (Th-²³⁵U)C, and (Th-²³⁵U)N at 300 MW_{th} power.

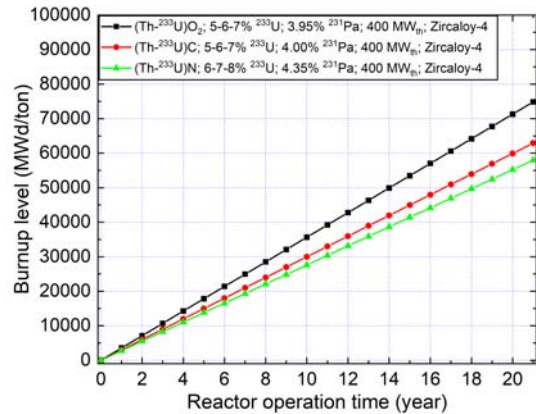


Fig. 13. Burnup level of (Th-²³⁵U)O₂, (Th-²³⁵U)C, and (Th-²³⁵U)N at 400 MW_{th} power.

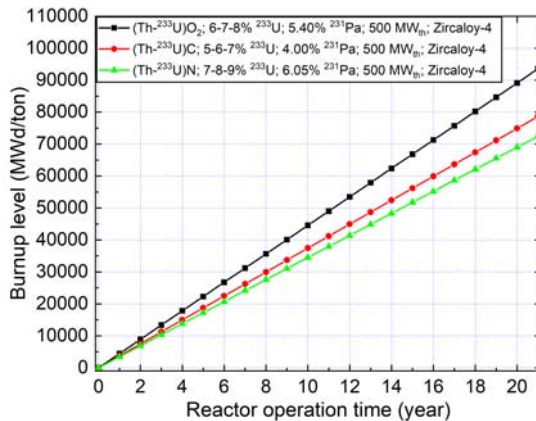


Fig. 14. Burnup level of (Th-²³⁵U)O₂, (Th-²³⁵U)C, and (Th-²³⁵U)N at 500 MW_{th} power.

effect on changes in burnup level. As shown in Figs. 12–14, the burnup level will increase as the reactor power increases. We can see that the highest burnup level for each power level is found in fuel (Th-²³⁵U)O₂, followed by (Th-²³⁵U)C, and the lowest burnup level is found in fuel type (Th-²³⁵U)N. For all power levels, it can be seen that the gradient of increase in burnup level for type fuels (Th-²³⁵U)C and (Th-²³⁵U)N is not much different, but the gradient of the rise in burnup level for fuel type (Th-²³⁵U)O₂ is more significant when compared to the other two types of fuel. The high burnup level for fuel type (Th-²³⁵U)O₂ is because the fuel has a lower density when compared to the other two types of fuel. The

higher the burnup level, the more the fuel efficiency improves and becomes more profitable. However, the high burnup level also demands more attention to technical issues. These include the increased accumulation of gaseous fission products within the fuel pin, which significantly increases the internal pressure and additional demands on the fuel cladding, which must withstand the reactor environment for extended periods [35, 36].




Conclusion

Neutronic studies have shown that (Th-²³⁵U)N fuel performs the best compared to other fuels regarding reactor criticality level. (Th-²³⁵U)N fuel with a ²³⁵U enrichment of 6–7–8% in the reactor core for both cladding types achieves critical conditions throughout the cycle with excess reactivity of <1.00% dk/k at 300 MW_{th} and 400 MW_{th} power levels. (Th-²³⁵U)C fuel can reach critical conditions throughout the cycle with excess reactivity <1.00% dk/k at a ²³⁵U configuration of 4–5–6% with zircaloy-4 cladding at a power level of 300 MW_{th}. Meanwhile, (Th-²³⁵U)O₂ fuel can reach critical conditions throughout the cycle but with a slightly higher excess reactivity exceeding 1.00% dk/k at a power level of 300 MW_{th} with a ²³⁵U enrichment configuration of 5–6–7% for both cladding types.

Neutronic studies reveal similar power density distribution patterns in the radial direction for (Th-²³⁵U)N and (Th-²³⁵U)C fuels, which are more evenly distributed compared to (Th-²³⁵U)O₂ fuel. Additionally, (Th-²³⁵U)O₂ fuel exhibits a relatively higher PPF than the other two fuels. The analysis indicates that fuel (Th-²³⁵U)N has the most negative Doppler coefficient on average, followed by (Th-²³⁵U)C and (Th-²³⁵U)O₂ fuels. Moreover, the burnup level analysis shows that (Th-²³⁵U)O₂ fuel has a significantly higher value than the other fuels, while (Th-²³⁵U)C fuel has a slightly higher burnup level than (Th-²³⁵U)N.

Acknowledgments. The author would like to acknowledge Lembaga Pengelola Dana Pendidikan (LPDP) – Ministry of Finance, the Republic of Indonesia, for supporting the first author by providing educational scholarships.

ORCID

B. P. Lapanporo  <http://orcid.org/0000-0002-0041-0427>
 A. P. A. Mustari  <http://orcid.org/0000-0002-6546-4493>
 Z. Su'ud  <http://orcid.org/0000-0001-8907-9824>

References

1. International Atomic Energy Agency. (2021). *Energy, electricity and nuclear power estimates for the period up to 2050*. Vienna: IAEA. (Reference Data Series no.

- 1). <https://www.iaea.org/publications/15028/energy-electricity-and-nuclear-power-estimates-for-the-period-up-to-2050>.
2. Cummins, W. E., & Matzie, R. (2018). Design evolution of PWRs: Shippingport to generation III+. *Prog. Nucl. Energy*, *102*, 9–37. DOI: 10.1016/j.pnucene.2017.08.008.
3. Rowinski, M. K., White, T. J., & Zhao, J. (2015). Small and medium sized reactors (SMR): A review of technology. *Renew. Sust. Energy Rev.*, *44*, 643–656. DOI: 10.1016/j.rser.2015.01.006.
4. Akbari-Jeyhouni, R., Rezaei Ochbelagh, D., Maiorino, J. R., D'Auria, F., & de Stefani, G. L. (2018). The utilization of thorium in small modular reactors – Part I: Neutronic assessment. *Ann. Nucl. Energy*, *120*, 422–430. DOI: 10.1016/j.anucene.2018.06.013.
5. Jagannathan, V., Mathur, A., & Khan, S. A. (2016). Thorium utilization in existing and advanced reactor types. *Int. J. Hydrog. Energy*, *41*(17), 7094–7102. DOI: 10.1016/j.ijhydene.2015.12.035.
6. du Toit, M. H., & Naicker, V. V. (2018). Neutronic design of homogeneous thorium/uranium fuel for 24 month fuel cycles in the European pressurized reactor using MCNP6. *Nucl. Eng. Des.*, *337*(5), 394–405. DOI: 10.1016/j.nucengdes.2018.07.023.
7. Tsige-Tamirat, H. (2011). Neutronics assessment of the use of thorium fuels in current pressurized water reactors. *Prog. Nucl. Energy*, *53*(6), 717–721. DOI: 10.1016/j.pnucene.2011.04.005.
8. Gorton, J. P., Collins, B. S., Nelson, A. T., & Brown, N. R. (2019). Reactor performance and safety characteristics of ThN-UN fuel concepts in a PWR. *Nucl. Eng. Des.*, *355*(7), 110317. DOI: 10.1016/j.nucengdes.2019.110317.
9. Trellue, H. R., Bathke, C. G., & Sadasivan, P. (2011). Neutronics and material attractiveness for PWR thorium systems using Monte Carlo techniques. *Prog. Nucl. Energy*, *53*(6), 698–707. DOI: 10.1016/j.pnucene.2011.04.007.
10. Subki, I., Pramutadi, A., Rida, S. N. M., Su'ud, Z., Eka Sapta, R., Nurul, S. Muh., Topan, S., Astuti, Y., & Soentono, S. (2008). The utilization of thorium for long-life small thermal reactors without on-site refueling. *Prog. Nucl. Energy*, *50*(2/6), 152–156. DOI: 10.1016/j.pnucene.2007.10.029.
11. Raj, D., & Kannan, U. (2022). Analysis for the use of thorium based fuel in LWRs. *Ann. Nucl. Energy*, *174*, 109162. DOI: 10.1016/j.anucene.2022.109162.
12. Humphrey, U. E., & Khandaker, M. U. (2018). Viability of thorium-based nuclear fuel cycle for the next generation nuclear reactor: Issues and prospects. *Renew. Sust. Energy Rev.*, *97*(8), 259–275. DOI: 10.1016/j.rser.2018.08.019.
13. Oettingen, M., & Cetnar, J. (2021). Numerical modeling of modular high-temperature gas-cooled reactors with thorium fuel. *Nukleonika*, *66*(4), 133–138. DOI: 10.2478/nuka-2021-0020.
14. Uguru, E. H., Sani, S. F. A., Khandaker, M. U., & Rabir, M. H. (2020). Investigation on the effect of ²³⁸U replacement with ²³²Th in small modular reactor (SMR) fuel matrix. *Prog. Nucl. Energy*, *118*(2), 103108. DOI: 10.1016/j.pnucene.2019.103108.
15. Galahom, A. A., Mohsen, M. Y. M., & Amrani, N. (2022). Explore the possible advantages of using

- thorium-based fuel in a pressurized water reactor (PWR). Part 1: Neutronic analysis. *Nucl. Eng. Technol.*, 54(1), 1–10. DOI: 10.1016/j.net.2021.07.019.
16. Oettingen, M., & Skolik, K. (2016). Numerical design of the Seed-Blanket Unit for the thorium nuclear fuel cycle. *E3S Web of Conf.*, 10, 3–7. DOI: 10.1051/e3sconf/20161000067.
 17. Liu, R., Cai, J., & Zhou, W. (2020). Multiphysics modeling of thorium-based fuel performance with a two-layer SiC cladding in a light water reactor. *Ann. Nucl. Energy*, 136, 107036. DOI: 10.1016/j.anucene.2019.107036.
 18. Castro, V. F., Velasquez, C. E., & Pereira, C. (2020). Criticality and depletion analysis of reprocessed fuel spiked with thorium in a PWR core. *Nucl. Eng. Des.*, 360(1), 110514. DOI: 10.1016/j.nucengdes.2020.110514.
 19. Tucker, L. P., & Usman, S. (2018). Thorium-based mixed oxide fuel in a pressurized water reactor: A burnup analysis with MCNP. *Ann. Nucl. Energy*, 111, 163–175. DOI: 10.1016/j.anucene.2017.08.057.
 20. Maiorino, J. R., Stefani, G. L., Moreira, J. M. L., Rossi, P. C. R., & Santos, T. A. (2017). Feasibility to convert an advanced PWR from UO₂ to a mixed U/ThO₂ core – Part I: Parametric studies. *Ann. Nucl. Energy*, 102, 47–55. DOI: 10.1016/j.anucene.2016.12.010.
 21. Zainuddin, N. Z., Parks, G. T., & Shwageraus, E. (2016). The factors affecting MTC of thorium-plutonium-fuelled PWRs. *Ann. Nucl. Energy*, 98, 132–143. DOI: 10.1016/j.anucene.2016.07.034.
 22. Morrison, S. L., Lindley, B. A., & Parks, G. T. (2018). Isotopic and spectral effects of Pu quality in Th-Pu fueled PWRs. *Ann. Nucl. Energy*, 117, 318–332. DOI: 10.1016/j.anucene.2018.03.025.
 23. Li, J., Li, X., & Cai, J. (2021). Neutronic characteristics and feasibility analysis of micro-heterogeneous duplex ThO₂-UO₂ fuel pin in PWR. *Nucl. Eng. Des.*, 382(3), 111382. DOI: 10.1016/j.nucengdes.2021.111382.
 24. Baldova, D., Fridman, E., & Shwageraus, E. (2016). High conversion Th-U233 fuel for current generation of PWRs: Part III – Fuel availability and utilization considerations. *Ann. Nucl. Energy*, 87, 517–526. DOI: 10.1016/j.anucene.2015.10.006.
 25. Duan, Z., Yang, H., Satah, Y., Murakami, K., Kano, S., Zhao, Z., Shen, J., & Abe, K. (2017). Current status of materials development of nuclear fuel cladding tubes for light water reactors. *Nucl. Eng. Des.*, 316, 131–150. DOI: 10.1016/j.nucengdes.2017.02.031.
 26. ARIS – Technical data. (2023). Vienna: International Atomic Energy Agency. <https://aris.iaea.org/sites/power.html> (accessed August 07, 2023).
 27. Lapanporo, B. P., & Su'Ud, Z. (2022). Parametric study of thorium fuel utilization on small modular pressurized water reactors (PWR). *J. Phys.-Conf. Series*, 2243(1). DOI: 10.1088/1742-6596/2243/1/012062.
 28. Okumura, K., Kugo, T., Kaneko, K., & Tsuchihashi, K. (2007). *SRAC2006: A comprehensive neutronics calculation code system*. Japan Atomic Energy Agency. DOI: 10.11484/JAEA-DATA-CODE-2007-004.
 29. Kulikov, G. G., Kulikov, E. G., Shmelev, A. N., & Apse, V. A. (2017). Protactinium-231 – New burnable neutron absorber. *Nucl. Energy Technol.*, 3(4), 255–259. DOI: 10.1016/j.nucet.2017.10.002.
 30. Bae, I. H., Na, M. G., Lee, Y. J., & Park, G. C. (2008). Calculation of the power peaking factor in a nuclear reactor using support vector regression models. *Ann. Nucl. Energy*, 35(12), 2200–2205. DOI: 10.1016/j.anucene.2008.09.004.
 31. Mohd Ali, N. S., Hamzah, K., Idris, F., Basri, N. A., Sarkawi, M. S., Sazali, M. A., Rabir, H., Minhat, M. S., & Zainal, J. (2022). Power peaking factor prediction using ANFIS method. *Nucl. Eng. Technol.*, 54(2), 608–616. DOI: 10.1016/j.net.2021.08.011.
 32. Kubiński, W., Darnowski, P., & Chęć, K. (2021). Optimization of the loading pattern of the PWR core using genetic algorithms and multi-purpose fitness function. *Nukleonika*, 66(4), 147–151. DOI: 10.2478/nuka-2021-0022.
 33. Ashiq, M., Ilyas, M., & Ahmad, S. U. I. (2016). Optimization of PWR design parameters for implementation in SMRs. *Ann. Nucl. Energy*, 94, 123–128. DOI: 10.1016/j.anucene.2015.12.015.
 34. Chen, C., Mei, H., He, M., & Li, T. (2022). Neutronics analysis of a 200 kWe space nuclear reactor with an integrated honeycomb core design. *Nucl. Eng. Technol.*, 54(12), 4743–4750. DOI: 10.1016/j.net.2022.08.012.
 35. Tverberg, T., & Wiesenack, W. (2002). Fission gas release and temperature data from XA0202217 instrumented high burnup LWR fuel. In *Technical and economic limits to fuel burnup extension* (pp. 7–16). Vienna: International Atomic Energy Agency. (IAEA-TECDOC-1299).
 36. Kiuchi, K., Ioka, I., Takizawa, M., & Wada, S. (2002). Development of advanced cladding material for burnup extension. In *Technical and economic limits to fuel burnup extension* (pp. 112–125). Vienna: International Atomic Energy Agency. (IAEA-TECDOC-1299).